Averaging of nuclear modulation artefacts in RIDME experiments

Originally published in:
Journal of Magnetic Resonance 272, https://doi.org/10.1016/j.jmr.2016.09.016

Averaging of nuclear modulation artefacts in RIDME experiments

Katharina Keller[a], Andrin Doll[a], Mian Qi[b], Adelheid Godt[b], Gunnar Jeschke[a], Maxim Yulikov[a,*]

[a] *Laboratory of Physical Chemistry, ETH Zurich, Vladimir-Prelog-Weg 2, CH-8093 Zurich, Switzerland*
[b] *Faculty of Chemistry and Center for Molecular Materials (CM$_2$), Bielefeld University, Universitätsstraße 25, 33615 Bielefeld, Germany*

Abstract

The presence of artefacts due to Electron Spin Echo Envelope Modulation (ESEEM) complicates the analysis of dipolar evolution data in Relaxation Induced Dipolar Modulation Enhancement (RIDME) experiments. Here we demonstrate that averaging over the two delay times in the refocused RIDME experiment allows for nearly quantitative removal of the ESEEM artefacts, resulting in potentially much better performance than the so far used methods. The analytical equations are presented and analyzed for the case of electron and nuclear spins $S = 1/2$, $I = 1/2$. The presented analysis is also relevant for Double Electron Electron Resonance (DEER) and Chirp-Induced Dipolar Modulation Enhancement (CIDME) techniques. The applicability of the ESEEM averaging approach is demonstrated on a Gd(III)-Gd(III) rigid ruler compound in deuterated frozen solution at Q band (35 GHz).

Keywords: RIDME, Q Band, electron spin envelope modulation suppression, EPR, paramagnetic metal ions, gadolinium

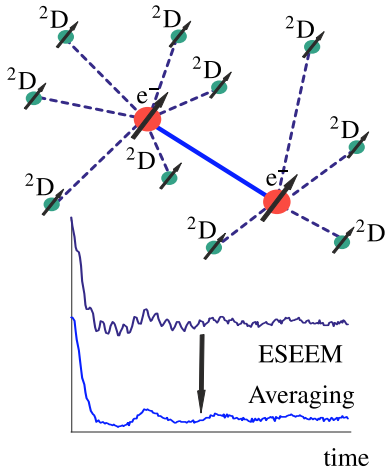

Site-specific distance measurements based on different types of pulse experiments in electron paramagnetic resonance (EPR) attract increasing interest in structural biology studies. [1–7] Pulse EPR provides the possibility of measuring long-distance constraints in the range between 2 and 10 nm, a range which is difficult to access by most other techniques. The approach that uses nitroxide radicals as spin labels and double electron-electron resonance (DEER) as the spectroscopic technique is currently the most popular one. [1, 3, 4, 7–10] However, a lot of effort has recently been invested to develop spin labels based on metal complexes, as well as trilateration approaches to determine positions of native transition metal centres in metalloproteins. [6, 11–21] In this context metal ions, such as Fe(III), Cu(II), Co(II), Mn(II), or Gd(III), attract attention. Paramagnetic metal ion-based spin labels have spectroscopic properties significantly different from those of nitroxides and other organic radicals, which makes them useful in orthogonal labeling approaches. [21] Furthermore, they may be able to withstand the reducing cell environment as proven for Gd(III). [22, 23]

Most metal centres exhibit broad EPR spectra, which in combination with the limited bandwidths of EPR microwave pulses give rise to low modulation depths in DEER experiments, thus decreasing the sensitivity. The two main approaches solving this problem are based on increasing the bandwidth for flipping the second spin in the dipolarly coupled spin pair. In the first approach this is achieved by applying a broad-band pump pulse, generated by an ultrafast arbitrary waveform generator. [14, 24, 25] The second approach, which offers nearly infinite effective bandwidth of the coupling partner, utilizes the longitudinal Relaxation Induced Dipolar Modulation Enhancement (RIDME) technique. [26–33] Being a single frequency technique, RIDME imposes low requirements on the resonator profile and measurement setup. On the downside, the RIDME time traces have typically faster decaying intermolecular background, as compared to DEER, and, for high-spin metal centres, also contain contributions of dipolar frequency overtones. Importantly, and unfortunately for measurement of dipole-dipole interactions, the RIDME technique is even more prone than DEER to unwanted Electron Spin Echo Envelope Modulation (ESEEM) effects, which introduce hyperfine frequencies to the dipolar evolution traces and thus interfere with distance measurements. This problem is less important at W band (94 GHz) or yet higher measurement frequencies, since at those conditions ESEEM contributions are usually weak and can be neglected in the majority of cases. However, at X and Q band (9.5 and 35 GHz) the ESEEM contributions from protons or deuterons (in deuterated solvents, or for deuterated biomolecules) make RIDME measurements significantly more difficult. The currently used approaches to avoid ESEEM arte-

*Corresponding author. Fax: +41-44 632 3118
Email address: maxim.yulikov@phys.chem.ethz.ch (Maxim Yulikov)

facts at these measurement frequencies lead to a loss of signal-to-noise ratio (SNR), since they are either based on the use of very soft microwave pulses or require trace by trace division. [27, 29, 30] The latter approach reduces signal-to-noise ratio by at least a factor of two, with a factor $\sqrt{2}$ coming from the requirement of measuring a reference trace that does not add to the dipolar modulation and another factor of $\sqrt{2}$ at the signal maximum and more at later time from dividing two noisy traces.

In this communication we describe an ESEEM averaging approach conceptually analogous to the one used in DEER spectroscopy, which allows using hard broadband pulses in RIDME measurements and does not require division of the RIDME trace by a reference. Importantly, the ESEEM averaging does not produce any distortions in the dipolar evolution traces, and does not significantly change the shape of the intermolecular background decay. Such an approach is of particular importance for measuring deuterated samples. Sample deuteration leads to much slower (flatter) intermolecular background decays in RIDME measurements and is recommended whenever possible to improve the quality of distance distribution curves. However, the amplitude of deuterium ESEEM is typically large in X-band and Q-band measurements, which made sample deuteration not very popular in RIDME-based studies to date.

We demonstrate our approach on frozen solutions in D_2O/glycerol-d_8 of mono-Gd(III) compound Gd-PyMTA and the Gd-ruler (3.4 nm), a di-Gd(III) compound with a most probable Gd-Gd distance of about 3.4 nm and a very narrow distance distribution, [34] shown in Figure 1. The pulse sequence of the dead time free RIDME experiment [27] is shown in Figure 1(a) and the echo detected (ED) EPR spectrum of the Gd(III)-PyMTA complex is shown in Figure 1(b) with the RIDME detection position marked by an arrow. Detailed experimental setting and sample preparation descriptions can be found in the Supporting Information.

Considering the formation of the RIDME echo, it is convenient to distinguish between A-spins, which are the spins excited by the microwave pulses, and B-spins, which are all other spins, in particular those, dipolar coupled to the A-spins within the same molecule. Using this terminology, the evolution of non-equilibrium magnetization in the RIDME pulse sequence (Figure 1(a)) can be described as follows. First, transverse magnetization is created for the A-spins by the $\pi/2$ pulse, it evolves for the time d_1, gets refocused by the π pulse and forms a spin echo at the time point $2d_1$. Next, the A-spins transverse magnetization starts to defocus again and at the time point $2d_1 + d_{12}$ half of it is transferred to the z-direction by the first $\pi/2$ pulse of the mixing block, thus forming a non- equilibrium polarization grid for A-spins along the direction of the external magnetic field. This grid is stored for the mixing time T_{mix}, to allow for spontaneous flips of the B-spins, resulting in a change of the dipole-dipole interaction, and thus shifting the resonance frequencies of the A-spins. After that the second $\pi/2$ pulse of the mixing block transfers the A-spins polarization back to the transverse plane. The resulting transverse magnetization evolves for the time d_2–d_{12}, is refocused by the last π pulse and forms the RIDME echo at time d_2 after the last π pulse. The time d_{12} is incremented, and the amplitude of the RIDME echo is recorded as a function of d_{12}.

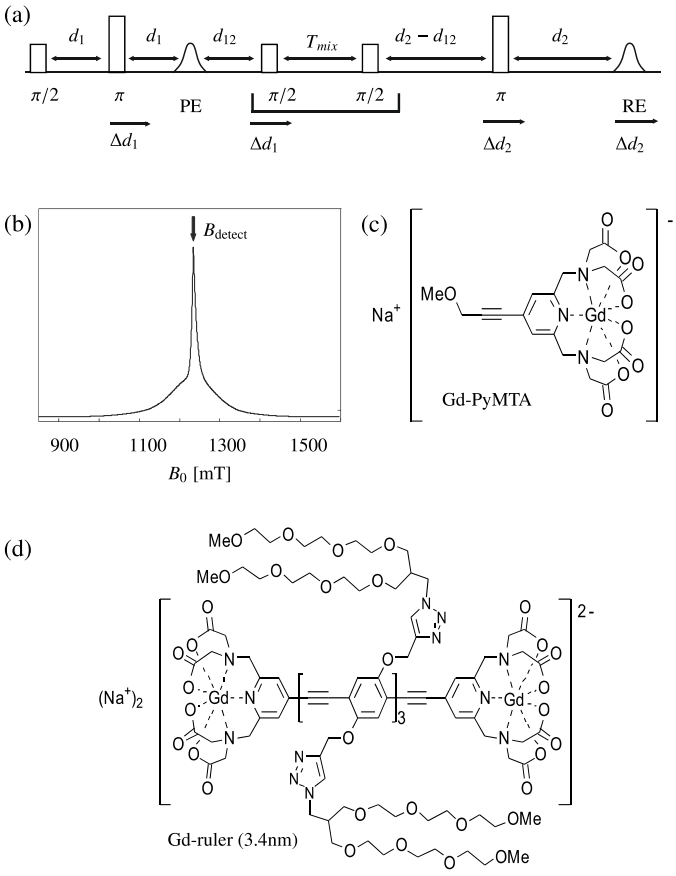

Figure 1: (a) RIDME pulse sequence, PE stands for the primary spin echo, and RE for the detected RIDME echo (refocused virtual echo in reference [27]), (b) EDEPR spectrum of the Gd-ruler (3.4 nm) at 34.5 GHz. The magnetic field position for detection of the RIDME sequence is marked by an arrow, (c), (d) Structural formulae of the studied model compounds.

The ESEEM effect appears as a modulation of the intensity of the electron spin echo due to the interaction of the electron spin with surrounding nuclei. [35] In a real experiment, in addition to the just described ideal pathway, each microwave pulse in the RIDME pulse sequence (Figure 1(a)) transfers electron coherence or polarization to electron-nuclear or pure nuclear coherence and polarization. As a result, the RIDME echo has contributions that oscillate with nuclear frequencies and combinations thereof by varying any delay time used in the experiment. An analytical computation of the propagation of coherence through the RIDME pulse sequence is provided in the Supporting Information. This computation was performed for an effective spin $S = 1/2$, which implies that we neglect any level crossing effects of the $S = 7/2$ spin of Gd(III). As long as this approximation is valid, our analysis of ESEEM averaging should be rather general and applicable to any paramagnetic centre, including low-spin and high-spin metal centres.

There are two time points in the RIDME sequence where all contributions to the detected RIDME echo (refocused virtual echo in [27]) assume a rather simple dependence on the

electron spin operators. First, at the primary echo time point $2d_1$ all contributions that later form the RIDME echo refocus along the y-direction. The RIDME signal has, therefore, the well known two-pulse ESEEM formula as a pre-factor , which is shown analytically in equation 5 in the SI. This two pulse ESEEM contribution in the RIDME signal has identical phase for any position of the mixing block, and, in principle, does not affect the dipolar evolution signal. The first refocusing π-pulse in the refocussed RIDME sequence [27] only serves as a tool for avoiding temporal overlap of the mixing block with excitation pulses and the dipolar evolution time. Therefore the nuclear modulation contribution of this block can be fully removed by averaging the RIDME echo signal over a range of d_1 times. The second time point, important for the formation of the RIDME signal, is the time right after the first $\pi/2$ pulse of the mixing block (third pulse in the refocused RIDME pulse sequence in Figure 1(a)). At this point the part of the transverse magnetization that is later detected as RIDME echo is turned into z-direction, creating electron polarization, electron-nuclear two-spin order (S_zI_z), and nuclear coherence and polarization, while all terms that are proportional to the S_x and S_y operators in the (xy) plane would nearly completely decay during the mixing time, which should be thus set at least 2-3 times longer than the electron phase memory time $T_{\mathrm{m,e}}$. The S_x and S_y terms are also suppressed by phase cycling. The polarization terms are constants of motion during the mixing time, while the phase of nuclear coherence evolves. All this terms are transferred back to the electron coherences by the second $\pi/2$ pulse of the mixing block, and participate in formation of the RIDME signal. Thus, there would be another factor in the RIDME signal that is essentially the same as the part of the three-pulse ESEEM formula that depends on the mixing time T_{mix} (see equations (6) and (7) in the SI). [35] At typical RIDME setup conditions, however, the mixing time is rather long and the terms that contain nuclear coherences, dephase or irreversibly decay over this period of time. Thus, in the majority of cases, the ESEEM oscillations during the mixing time do not affect the RIDME measurement and can be dropped in analytical computations. In the Supporting Information these terms are still considered for the sake of completeness.

The remaining evolution periods from the primary echo until the beginning of the mixing block, from the end of the mixing block until the last, refocusing π pulse, and from this last pulse until the position of the RIDME echo, produce further oscillatory terms with the properties of the transverse evolution part of the three-pulse ESEEM experiment, additionally refocused, as well as the ones of another two-pulse ESEEM block. In the equations given in the Supporting Information one can recognize that the majority of the terms either depend on the time d_2 (time delay between the last π-pulse and the RIDME echo, see Fig. 1(a)), or on the sum or difference of the time d_{12} (the time between the primary echo and the beginning of the mixing block, Fig. 1(a)) and the time d_2. All these terms are averaged out by varying the second static delay d_2 in the RIDME experiment. There are still two terms ($cos(d_{12}\omega_\alpha) + \cos(d_{12}\omega_\beta)$, see Supporting Information) left after such averaging that depend solely on the d_{12} time and are thus not averaged out. The overall pre-factor for these terms is $k/(8-6k)$ times smaller than the constant term, which is a rather small number for most values of k. Here $k = \left(\frac{B\omega_I}{\omega_\alpha\omega_\beta}\right)$ is the modulation depth parameter, B the pseudo-secular hyperfine coupling, ω_I the nuclear Zeeman frequency and ω_α, ω_β the nuclear frequencies in the spin-manifolds α, β. [35]

If we consider the 'worst' cases with $k \approx 1$, which can appear at X-Band for ^2D ESEEM, the remaining non-averaged ESEEM oscillations have an amplitude of about 50% of the total echo intensity. At Q band, where for deuterons the value of k is typically less than 0.1 these remaining ESEEM contributions have an amplitude of about 1.3% or less and do not affect the dipolar measurements to a significant extent in most applications, except for cases with very low spin labeling efficiencies when the RIDME modulation depth decreases to a level of 1-2% of the total echo intensity. Note that at typical lengths of d_2 of RIDME traces of one to several microseconds, the ESEEM modulation depths are actually smaller than the mentioned maximum values, so that a stronger suppression of the ESEEM artefacts due to the d_2 averaging would be expected even at X band.

Note further that the RIDME mixing block can be considered as a composite π-pulse. Such a π-pulse is, of course, applied at the same frequency as the detection pulses, but it produces ESEEM artefacts in a similar way as the pump pulse in the DEER experiment, which is applied at a different frequency but typically still slightly overlaps with the detection pulses in the frequency domain. This bandwidth overlap in DEER can be controlled by the pump-detection frequency offset and the pulse power settings. The main difference between the DEER pump and 'RIDME' composite pulse is thus the much stronger bandwidth overlap between the 'composite π-pulse' and the detection pulses of RIDME in comparison to the bandwidth overlap in DEER. This overlap makes ESEEM artefacts stronger in the RIDME case. The effect of spontaneous spin flips is analogous to the effect of a chirp pulse applied during the mixing block of the Chirp-Induced Dipolar Modulation Enhancement (CIDME) experiment. [36] Our analytical treatment of the ESEEM averaging would be thus relevant also for DEER and CIDME techniques.

We have experimentally tested the performance of the ESEEM averaging scheme based on the above analysis. Considering the structure of the compound (Figure 1), solvent, and chosen microwave frequency (35 GHz), mainly nuclear modulation from ^{2}D nuclei of about 7.8 MHz (at 1200 mT) is expected and can be identified in the primary data in figure 2 (top, purple line). The following time steps and durations of the averaging period, thus, directly apply to the deuterium nuclear modulations at Q band, and should be adjusted accordingly for other nuclei and detection frequencies. Note also that in cases of ESEEM oscillations originating from two or more types of nuclei, more extended ESEEM averaging schemes might appear necessary.

The principle of the averaging scheme is sketched in figure 1. It can be considered as two two-pulse ESEEM like blocks consisting of the characteristic $\pi/2$-π pulses and interpulse de-

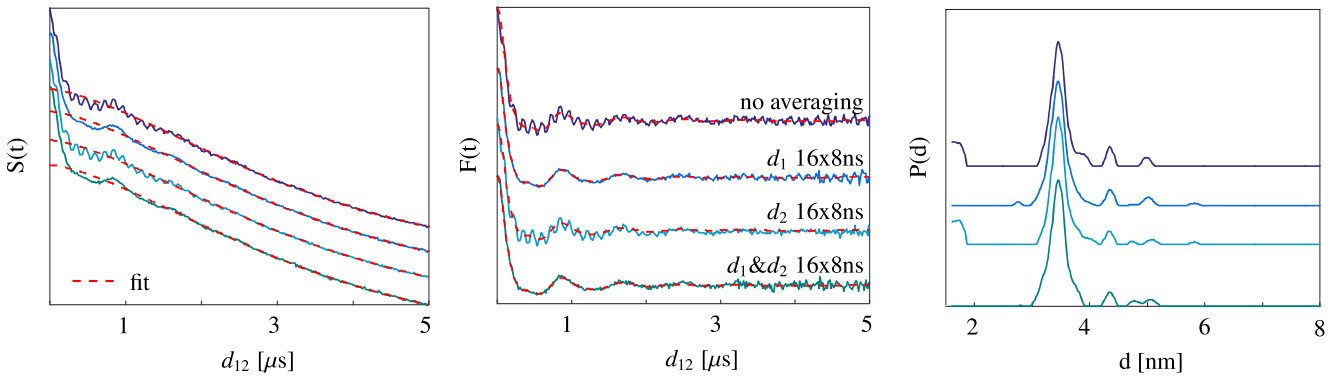

Figure 2: Q-Band RIDME spectra for the Gd-ruler (3.4 nm) at 20 K showing different averaging schemes. From left to right: primary data, form factor and distance distribution.

lay d_1, d_2, respectively. In this framework, both building blocks will introduce nuclear modulations in the primary data. To suppress the generated nuclear modulations, the RIDME traces are acquired for several d_1, d_2 pairs, starting from the initial values and increasing the delays in steps of Δd_1 and Δd_2. Eventually all traces are summed up. Averaging of the first interpulse delay d_1 ($\Delta d_2 = 0$) already results in a drastic decrease of the deuteron ESEEM modulations (blue, second top line). Nevertheless, small ESEEM oscillations can be observed towards the end of the trace. These can be suppressed by averaging the second interpulse delay d_2 ($\Delta d_1 = 0$) (third top, cyan line), yet strong deuterium oscillations remain at the beginning of the traces. Averaging of both interpulse delays ($\Delta d_1 = \Delta d_2$) suppresses the deuterium ESEEM effect to a level below the noise if the averaging period exceeds 128 ns (bottom, yellow line). It should be noted that for very short mixing times $T_{\mathrm{mix}} < T_m$ an additional oscillating term, dependent on T_{mix} plays a role as shown in Figure S.1 in the Supporting Information. This term, however, becomes unimportant at longer mixing times ($\sim 2T_m$) due to nuclear coherence decay.

Importantly, the averaging approach does not change the primary RIDME signal or the RIDME form factor. Tikhonov regularization thus results in alike distance distributions. Small differences are observed in the artefact peaks. Especially incomplete averaging of the fast oscillations in the beginning of the trace induces a short distance artefact, while incomplete averaging towards the end of the trace introduces some small changes in the long-range artefact level around 5 nm.

The mean signal intensity of the RIDME background traces is shown for Gd(III)-PyMTA as a function of Δd_1 with $\Delta d_1 = \Delta d_2$ in Figure 3(a). It exhibits the typical cos-like amplitude oscillation [35] of nuclear modulation, while the contribution of the unmodulated part remains constant with increasing interpulse delay (in practice, slowly decays, mainly due to the spectral diffusion). As estimated from the ^{2}D Larmor frequency, a full period of oscillation is approximately 128 ns. We found (figure 3(b)) that by averaging of the RIDME time traces by increasing d_1, d_2 pairs, only the unmodulated part of the signal decay remains, while its shape is not distorted. These experiments on a mono-gadolinium compound show no change in the RIDME background upon application of such ESEEM averaging procedures.

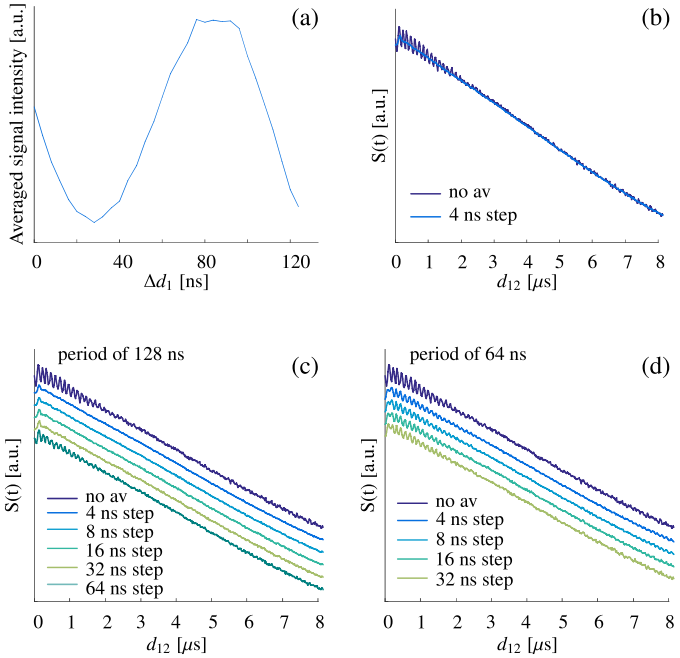

Figure 3: Q-Band RIDME data for Gd-PyMTA ligand acquired at 20K. a) Mean intensity of the primary RIDME traces as a function of Δd_1 with $\Delta d_1 = \Delta d_2$. b) Comparison of unprocessed primary data to a summation of all traces. c) Averaging of traces with increasing step size from top to bottom for a period of 128 ns. d) Averaging of traces with increasing step size from top to bottom for a period of 64 ns.

Figure 3(c, d) shows the influence of averaging period and spacing Δd_1, Δd_2 on the quality of ESEEM artefact removal. It can be concluded that the averaging approach is rather insensitive to the applied step size up to the step of 32 ns corresponding to roughly a quarter of the total oscillation period. On the other hand, at least one full period of nuclear modulation needs to be detected (figure 3(c)). Averaging only half a period (64 ns) of the deuterium modulation (figure 3(d)) results in a reduction of the ESEEM effect, but not in full suppression. Nevertheless, the level of reduction remains constant within a step size of 32 ns. Note that averaging with more steps does not reduce signal-to-

noise ratio, since all traces contribute the full dipolar modulation. A larger number of steps merely increases the minimum duration of the experiment. Some signal loss occurs since the average d_1 and d_2 intervals are larger than would be required without nuclear modulation averaging. With a total averaging interval of 256 ns in deuterated samples this loss is moderate for the typical transverse relaxation times, where RIDME can be measured.

To summarize, we have demonstrated that introduction of an ESEEM averaging loop in the RIDME measurement protocol efficiently removes the electron-nuclear interaction artefacts and allows obtaining clean dipolar time traces at Q band. Importantly, the averaging on two delay times (d_1 and d_2) as well as varying of the delay times by at least one full period of ESEEM oscillations is crucial for obtaining clean data. The proposed averaging procedure does not reveal any detectable changes in the RIDME form factor and background decay, thus leading to no influence on the distance analysis. Important advantages of the described procedure are that no reference measurement is required and that microwave pulses of arbitrary bandwidths can be used. Therefore signal-to-noise ratio is generally improved as compared to the previously suggested ESEEM removal procedures. [27, 29, 30] While the experiments presented here were performed at Q band, the approach is expected to work with a similar efficiency at any other relevant microwave band for comparable depths of ESEEM oscillations. However, due to the incomplete nuclear modulation averaging, the performance of the proposed approach is expected to be worse for particularly strong ESEEM modulation depths, which are typical for low detection frequencies and for strongly coupled nuclei. We believe that such an ESEEM averaging procedure will simplify the use of the RIDME technique for the distance measurements in biomacromolecules.

Acknowledgements

Authors acknowledge financial support of the Swiss National Science Foundation (Grants No. SNF 200020_14441 and 200020_157034/1) and the Deutsche Forschungsgemeinschaft (SPP1601, GO 555/6-2).

References

[1] G. Jeschke, Y. Polyhach, Distance measurements on spin-labelled biomacromolecules by pulsed electron paramagnetic resonance, Phys. Chem. Chem. Phys. 9 (16) (2007) 1895–1910. doi:10.1039/B614920K.

[2] O. Schiemann, T. F. Prisner, Long-range distance determinations in biomacromolecules by EPR spectroscopy, Quarterly Reviews of Biophysics 40 (01) (2007) 1–53. doi:10.1017/S003358350700460X.

[3] J. P. Klare, H.-J. Steinhoff, Spin labeling EPR, Photosynthesis Research 102 (2) (2009) 377–390. doi:10.1007/s11120-009-9490-7.

[4] E. Bordignon, Site-directed spin labeling of membrane proteins., Top Curr Chem 321 (2012) 121–157. doi:10.1007/128_2011_243.

[5] I. Krstic, B. Endeward, D. Margraf, A. Marko, T. F. Prisner, Structure and Dynamics of Nucleic Acids, Top Curr Chem 321 (2012) 159–198. doi:10.1007/128_2011_300.

[6] G. Jeschke, DEER distance measurements on proteins., Annu Rev Phys Chem 63 (2012) 419–446. doi:10.1146/annurev-physchem-032511-143716.

[7] W. L. Hubbell, C. J. Lopez, C. Altenbach, Z. Yang, Technological advances in site-directed spin labeling of proteins., Curr Opin Struct Biol 23 (5) (2013) 725–733. doi:10.1016/j.sbi.2013.06.008.

[8] G. E. Fanucci, D. S. Cafiso, Recent advances and applications of site-directed spin labeling., Curr Opin Struct Biol 16 (5) (2006) 644–653. doi:10.1016/j.sbi.2006.08.008.

[9] M. Pannier, S. Veit, A. Godt, G. Jeschke, H. Spiess, Dead-Time Free Measurement of Dipole–Dipole Interactions between Electron Spins, Journal of Magnetic Resonance 142 (2) (2000) 331–340. doi:10.1006/jmre.1999.1944.

[10] G. Jeschke, A. Koch, U. Jonas, A. Godt, Direct conversion of EPR dipolar time evolution data to distance distributions., J Magn Reson 155 (1) (2002) 72–82. doi:10.1006/jmre.2001.2498.

[11] Z. Yang, J. Becker, S. Saxena, On Cu(II)-Cu(II) distance measurements using pulsed electron electron double resonance., J Magn Reson 188 (2) (2007) 337–343. doi:10.1016/j.jmr.2007.08.006.

[12] M. Ji, S. Ruthstein, S. Saxena, Paramagnetic metal ions in pulsed ESR distance distribution measurements., Acc Chem Res 47 (2) (2014) 688–695. doi:10.1021/ar400245z.

[13] B. E. Bode, J. Plackmeyer, T. F. Prisner, O. Schiemann, PELDOR measurements on a nitroxide-labeled Cu(II) porphyrin: orientation selection, spin-density distribution, and conformational flexibility., J Phys Chem A 112 (23) (2008) 5064–5073. doi:10.1021/jp710504k.

[14] P. E. Spindler, S. J. Glaser, T. E. Skinner, T. F. Prisner, Broadband inversion PELDOR spectroscopy with partially adiabatic shaped pulses., Angew Chem Int Ed Engl 52 (12) (2013) 3425–3429. doi:10.1002/anie.201207777.

[15] A. Doll, M. Qi, S. Pribitzer, N. Wili, M. Yulikov, A. Godt, G. Jeschke, Sensitivity enhancement by population transfer in Gd(III) spin labels., Phys Chem Chem Phys 17 (11) (2015) 7334–7344. doi:10.1039/c4cp05893c.

[16] A. M. Raitsimring, C. Gunanathan, A. Potapov, I. Efremenko, J. M. L. Martin, D. Milstein, D. Goldfarb, Gd3+ complexes as potential spin labels for high field pulsed EPR distance measurements., J Am Chem Soc 129 (46) (2007) 14138–14139. doi:10.1021/ja075544g.

[17] P. Lueders, G. Jeschke, M. Yulikov, Double Electron-Electron Resonance Measured Between Gd3+ Ions and Nitroxide Radicals, J. Phys. Chem. Lett. 2 (6) (2011) 604–609. doi:10.1021/jz200073h.

[18] M. Yulikov, P. Lueders, M. F. Warsi, V. Chechik, G. Jeschke, Distance measurements in Au nanoparticles functionalized with nitroxide radicals and Gd(3+)-DTPA chelate complexes., Phys Chem Chem Phys 14 (30) (2012) 10732–10746. doi:10.1039/c2cp40282c.

[19] B. Joseph, V. M. Korkhov, M. Yulikov, G. Jeschke, E. Bordignon, Conformational cycle of the vitamin B12 ABC importer in liposomes detected by double electron-electron resonance (DEER)., J Biol Chem 289 (6) (2014) 3176–3185. doi:10.1074/jbc.M113.512178.

[20] D. Goldfarb, Gd3+ spin labeling for distance measurements by pulse EPR spectroscopy., Phys Chem Chem Phys 16 (21) (2014) 9685–9699. doi:10.1039/c3cp53822b.

[21] M. Yulikov, Chapter 1 Spectroscopically orthogonal spin labels and distance measurements in biomolecules, Electron Paramag Reson 24 (2015) 1–31.

[22] M. Qi, A. Groß, G. Jeschke, A. Godt, M. Drescher, Gd(III)-PyMTA Label Is Suitable for In-Cell EPR, J. Am. Chem. Soc. 136 (43) (2014) 15366–15378. doi:10.1021/ja508274d.

[23] A. Martorana, G. Bellapadrona, A. Feintuch, E. Di Gregorio, S. Aime, D. Goldfarb, Probing Protein Conformation in Cells by EPR Distance Measurements using Gd3+ Spin Labeling, J. Am. Chem. Soc. 136 (38) (2014) 13458–13465. doi:10.1021/ja5079392.

[24] A. Doll, S. Pribitzer, R. Tschaggelar, G. Jeschke, Adiabatic and fast passage ultra-wideband inversion in pulsed EPR, Journal of Magnetic Resonance 230 (2013) 27–39. doi:10.1016/j.jmr.2013.01.002.

[25] A. Doll, M. Qi, N. Wili, S. Pribitzer, A. Godt, G. Jeschke, Gd(III)-Gd(III) distance measurements with chirp pump pulses., J Magn Reson 259 (2015) 153–162. doi:10.1016/j.jmr.2015.08.010.

[26] L. Kulik, S. Dzuba, I. Grigoryev, Y. Tsvetkov, Electron dipole–dipole interaction in ESEEM of nitroxide biradicals, Chemical Physics Letters 343 (3–4) (2001) 315–324. doi:10.1016/S0009-2614(01)00721-7.

[27] S. Milikisyants, F. Scarpelli, M. G. Finiguerra, M. Ubbink, M. Huber, A pulsed EPR method to determine distances between paramagnetic centers with strong spectral anisotropy and radicals: The dead-time free RIDME

sequence, Journal of Magnetic Resonance 201 (1) (2009) 48–56. doi:10.1016/j.jmr.2009.08.008.

[28] S. Razzaghi, M. Qi, A. I. Nalepa, A. Godt, G. Jeschke, A. Savitsky, M. Yulikov, RIDME Spectroscopy with Gd(III) Centers., J Phys Chem Lett 5 (22) (2014) 3970–3975. doi:10.1021/jz502129t.

[29] D. Abdullin, F. Duthie, A. Meyer, E. S. Muller, G. Hagelueken, O. Schiemann, Comparison of PELDOR and RIDME for Distance Measurements between Nitroxides and Low-Spin Fe(III) Ions., J Phys Chem B 119 (43) (2015) 13534–13542. doi:10.1021/acs.jpcb.5b02118.

[30] A. V. Astashkin, Chapter Ten - Mapping the Structure of Metalloproteins with RIDME, in: Peter Z. Qin and Kurt Warncke (Ed.), Methods in Enzymology, Vol. Volume 563, Academic Press, 2015, pp. 251–284.

[31] A. Meyer, D. Abdullin, G. Schnakenburg, O. Schiemann, Single and double nitroxide labeled bis(terpyridine)-copper(ii): influence of orientation selectivity and multispin effects on PELDOR and RIDME, Phys. Chem. Chem. Phys. 18 (13) (2016) 9262–9271. doi:10.1039/C5CP07621H.

[32] A. Meyer, O. Schiemann, PELDOR and RIDME Measurements on a High-Spin Manganese(II) Bisnitroxide Model Complex, J. Phys. Chem. A 120 (20) (2016) 3463–3472. doi:10.1021/acs.jpca.6b00716.

[33] A. Collauto, V. Frydman, M. D. Lee, E. H. Abdelkader, A. Feintuch, J. D. Swarbrick, B. Graham, G. Otting, D. Goldfarb, RIDME distance measurements using Gd(III) tags with a narrow central transition, Phys. Chem. Chem. Phys.doi:10.1039/C6CP03299K.

[34] A. Dalaloyan, M. Qi, S. Ruthstein, S. Vega, A. Godt, A. Feintuch, D. Goldfarb, EPR distance measurements – the range of accessible distances and the impact of zero field splitting, Phys. Chem. Chem. Phys. 17 (28) (2015) 18464–18476. doi:10.1039/C5CP02602D.

[35] A. Schweiger, G. Jeschke, Principles of pulse electron paramagnetic resonance., Oxford University Press, 2001.

[36] A. Doll, Frequency-swept microwave pulses for electron spin resonance, Ph.D. thesis, ETH Zurich (2016).